Letters

A Fast and Efficient Two-Step Open Phase Fault Diagnostic Method for Dual Three-Phase PMSMs Using Harmonic Components

Zhe Tong, *Student Member, IEEE*, Yuting Lu, *Student Member, IEEE*, Beichen Ding, *Member, IEEE*, and Guodong Feng, *Senior Member, IEEE*

***Abstract*—This letter proposes a fast and efficient open phase fault (OPF) diagnostic method using the harmonic components for dual three-phase permanent magnet synchronous machines (PMSMs). The diagnosis consists of fault detection and localization, in which the indicator based on fourth harmonic is derived to detect whether OPF happens, and the indicator based on second harmonic is derived to locate the OPF. This two-step fault diagnostic method can locate the fault within 1/5 electrical cycle, which is fast and computation-efficient. Moreover, it does not depend on motor parameters and is robust to operating condition change. Compared with existing methods, the proposed method is applicable to both surface-mounted and interior motors with various control strategies. Experiments and comparisons are conducted to validate the performance of the proposed method.**

***Index Terms*—Current harmonics, dual three-phase permanent magnet synchronous machine (DT-PMSM), fault diagnosis, harmonic extraction, open phase fault (OPF), two-step strategy.**

I. Introduction

DUAL three-phase permanent magnet synchronous machines (DT-PMSMs) have great application potential in ships, aircraft and electric vehicles due to higher reliability, less power stress per phase and better fault-tolerant capability [1], [2], [3]. Many factors, such as long running, overheat and illegal operations, could lead to various faults in DT-PMSM. Among these faults, open phase fault (OPF) is common, which could induce the torque ripple, additional loss and even irreversible damage to the system [4], [5]. Thus, it is crucial to diagnose the fault quickly for the safety of DT-PMSM drive.

Received 28 March 2025; revised 28 April 2025; accepted 12 May 2025. Date of publication 15 May 2025; date of current version 30 June 2025. This work was supported in part by the National Natural Science Foundation of China under Grant 62473387, in part by the Southern Marine Science and Engineering Guangdong Laboratory (Zhuhai) under Grant SML2023SP241, and in part by the Department of Science and Technology of Guangdong Province under Grant 2021QN020085. *(Corresponding author: Beichen Ding.)*

Zhe Tong, Yuting Lu, and Guodong Feng are with the School of Intelligent Systems Engineering & Southern Marine Science and Engineering Guangdong Laboratory (Zhuhai), Sun Yat-sen University, Haizhu 510275, China (e-mail: tongzh@mail2.sysu.edu.cn; luyt28@mail2.sysu.edu.cn; fenggd6@mail.sysu.edu.cn).

Beichen Ding is with the School of Advanced Manufacturing & Southern Marine Science and Engineering Guangdong Laboratory (Zhuhai), Sun Yat-sen University, Haizhu 510275, China (e-mail: dingbch@mail.sysu.edu.cn).

Color versions of one or more figures in this article are available at https://doi.org/10.1109/TPEL.2025.3570693.

Digital Object Identifier 10.1109/TPEL.2025.3570693

OPF diagnostic methods mainly contain model-based methods, data-based methods and signal-based methods. The model-based methods utilize the residuals between the predicted and measured outputs to detect faults. These methods usually focus on the design of prediction models. For example, in [6], an interval sliding mode observer is applied for the fault detection. In [7], the model predictive control is combined with the mixed logical dynamic model to improve the accuracy. However, due to parameter variation in practical applications, the diagnostic performance of model-based methods is limited.

Based on the artificial intelligence algorithms, the data-based methods construct the fault classification models for fault diagnosis. In [8], the average values of phase currents are chosen as input features of the support vector machine for the fault detection. In practical applications, it is hard to obtain large amount of training samples under fault conditions. Thus, [9] employs the wavelet convolutional neural network to achieve fault diagnosis, which only requires small samples. Besides, an attribute matching based small-sample diagnostic method is proposed [10]. In [11], a clustering-based learning model is proposed to solve small sample and unknown fault problems. In [19], wavelet transform and mask impute are used to reduce the computation, and data normalization is developed in [20] to improve the robustness. Although the data-based methods are effective and robust, the computation is complex and the diagnosis usually needs more than one electrical cycle.

The signal-based methods design the indicators based on the measured signals to achieve fault diagnosis. Depending on the measured signals, the methods can be divided into voltage-based methods and current-based methods. The voltage-based methods can achieve fast fault diagnosis. For instance, through the high and low frequency voltages, Feng et al. [21] achieve accurate and reliable fault diagnosis. In [12], the fault is diagnosed in 1/20 electrical cycle, but the voltage-based methods need additional sensors. In order to avoid additional sensors, current-based methods are widely researched. Liu et al. [22] consider the feedback regulation of the controller and proposes an accurate fault detection method using current bias. Moreover, Zhao et al. [23] analyze the spatial distributions of phase currents and designs two indicators for fault localization. However, the current-based methods need more time for the diagnosis. For example, Zheng et al. [15] and Wang et al. [16] need two

electrical cycles and one electrical cycle, respectively. And the robustness could be affected by the current harmonics [13]. Moreover, Guo et al. [14] can diagnose the fault within 1/4 electrical cycle, but it limits to $i_d = 0$ control.

This letter proposes a fast and efficient two-step OPF diagnostic method based on the current harmonics in rotating frame. The diagnostic process is divided into two steps to improve the computation efficiency. In the fault detection, the phase difference of 4th current harmonic is chosen as the indicator. In the fault localization, the phase of second current harmonic is used to locate the faulty phase. Using the harmonics, the fault can be diagnosed within 1/5 electrical cycle. And the proposed method is robust and applicable to various control strategies for surface-mounted and interior motors. The experiments and comparisons are conducted on a test motor to validate the speed, robustness and effectiveness of the proposed method.

II. Modeling of DT-PMSM Under OPF

In this letter, the DT-PMSM has two sets of three-phase windings, which are denoted as (*A*, *B*, *C*) and (*D*, *E*, *F*) and are spatially shifted by $\pi/6$ with two isolated neutral points. The currents in different frames are denoted as

$$\begin{cases} \boldsymbol{i}_{s,f} = \begin{bmatrix} i_{A,f} & i_{B,f} & i_{C,f} & i_{D,f} & i_{E,f} & i_{F,f} \end{bmatrix}^{\mathrm{T}} \\ \boldsymbol{i}_{dq,f} = \begin{bmatrix} i_{d1,f} & i_{q1,f} & i_{d2,f} & i_{q2,f} \end{bmatrix}^{\mathrm{T}} \end{cases} \tag{1}$$

where $\boldsymbol{i}_s$ and $\boldsymbol{i}_{dq}$ denote the current vectors in the *ABCDEF* and dq_{12} frames, respectively; the subscript "$_f$" denotes that the currents are under fault. Under fault condition, the relationships of currents in different frames are defined as

$$\boldsymbol{i}_{dq,f} = \boldsymbol{T}_R \boldsymbol{T}_{VSD} \boldsymbol{i}_{s,f} = \boldsymbol{T}_{dq} \boldsymbol{i}_{s,f} \tag{2}$$

where $\boldsymbol{T}_{\mathrm{VSD}}$ and $\boldsymbol{T}_R$ are VSD and rotating matrixes given in Appendix I, respectively; and $\boldsymbol{T}_{dq} = \boldsymbol{T}_R \boldsymbol{T}_{\mathrm{VSD}}$.

Under OPF, $\boldsymbol{i}_{s,f}$ should satisfy some constraints. For example, when the phase *D* is open, the current in phase *D* is zero. Due to isolated neutral points, $\boldsymbol{i}_{s,f}$ satisfies

$$i_{A,f} + i_{B,f} + i_{C,f} = 0, i_{D,f} = 0, i_{E,f} = -i_{F,f}. \tag{3}$$

Without loss of generality, the OPF in phase *D* is studied as an example, and results for OPF in other phases are given directly.

III. Two-Step Fault Diagnostic Method Using Harmonic Components for DT-PMSM

As shown in Fig. 1, the proposed two-step fault diagnostic method consists of fault detection and localization. In the first step, the fourth order current harmonic is used to detect whether the fault occurs in (*A*, *B*, *C*) or (*D*, *E*, *F*), and in the second step, the faulty phase is located using the second order current harmonic. Through using high order harmonics, the proposed method can improve the diagnostic speed and computation efficiency as well as enhancing the robustness.

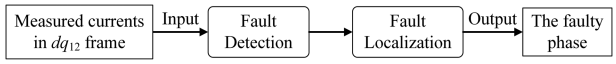

Fig. 1. Overview of proposed two-step fault diagnostic method.

A. Fault Detection

The fourth current harmonic in dq_{12} frame can be detected from the measurements and is employed to quickly detect whether the fault occurs. The fourth current harmonic vector is denoted as

$$\begin{bmatrix} i_{q1,4\mathrm{th}} \\ i_{d2,4\mathrm{th}} \end{bmatrix} = \begin{bmatrix} I_{q1,4\mathrm{th}} \cos\left(4\theta - \varphi_{q1,4\mathrm{th}}\right) \\ I_{d2,4\mathrm{th}} \cos\left(4\theta - \varphi_{d2,4\mathrm{th}}\right) \end{bmatrix} \tag{4}$$

where I_{dq12} and φ_{dq12} denote the amplitudes and phases; the subscript "$_{4\mathrm{th}}$" denotes fourth harmonic; θ is the rotor position. The difference between $\varphi_{q1,4\mathrm{th}}$ and $\varphi_{d2,4\mathrm{th}}$ is chosen to detect OPF, which is defined as

$$\Delta\varphi \triangleq \left|\varphi_{q1,4\mathrm{th}} - \varphi_{d2,4\mathrm{th}}\right|. \tag{5}$$

When phase *D* is open, in order to obtain $\Delta\varphi$, consider third and fifth harmonics in the phases *E* and *F*, which are denoted as

$$\begin{aligned} \boldsymbol{i}_{s,3,5} = \big[\boldsymbol{0}_{1\times 4} \quad & \cos\left(3\theta - \varphi_3\right) + \cos\left(5\theta - \varphi_5\right) \\ & - \cos\left(3\theta - \varphi_3\right) - \cos\left(5\theta - \varphi_5\right)\big]^{\mathrm{T}} \end{aligned} \tag{6}$$

where $\boldsymbol{i}_{s,3,5}$ is the current harmonic vector; φ_3 and φ_5 are the phases of corresponding harmonics.

Remark: In (6), the amplitudes of harmonics have same effect on $\varphi_{q1,4\mathrm{th}}$ and $\varphi_{d2,4\mathrm{th}}$, so $\Delta\varphi$ is not affected by the amplitudes. To simplify the equations, the amplitudes are set to 1. Moreover, the harmonics in phase *A*, *B*, and *C* do not contribute to $i_{q1,4\mathrm{th}}$ and $i_{d2,4\mathrm{th}}$, which is proven in Appendix II.

Substituting (6) into (2), the harmonic currents in q_1 and d_2 axes can be derived as (7) shown at the bottom of this page, where $\varphi_{+3} = \varphi_3 + \pi/3$, $\varphi_{-3} = \varphi_5 - \pi/3$, $\varphi_- = (\varphi_5 - \varphi_3)/2$, $\varphi_+ = (\varphi_5 + \varphi_3)/2$; the subscript "$_{2,4,6}$" denotes second, fourth, and sixth harmonics. Extracting the fourth harmonic from (7), one can obtain

$$\begin{bmatrix} i_{q1,4\mathrm{th}} \\ i_{d2,4\mathrm{th}} \end{bmatrix} = \frac{\sqrt{3}}{3} \begin{bmatrix} \sin\left(\varphi_- + \pi/3\right)\cos\left(4\theta - \varphi_+\right) \\ \sin\left(\varphi_- + \pi/3\right)\cos\left(4\theta - \varphi_+ - \pi\right) \end{bmatrix}. \tag{8}$$

Thus, when the phase *D* is open, we can observe

$$\Delta\varphi = \left|\varphi_+ - \varphi_+ - \pi\right| = \pi. \tag{9}$$

Based on similar derivation, $\Delta\varphi$ under OPF satisfies

$$\Delta\varphi = \begin{cases} 0 & \text{when } A, B \text{ or } C \text{ is opened} \\ \pi & \text{when } D, E \text{ or } F \text{ is opened} \end{cases}. \tag{10}$$

$$\begin{aligned} \begin{bmatrix} i_{q1,2,4,6} \\ i_{d2,2,4,6} \end{bmatrix} &= \frac{\sqrt{3}}{3}\left[\cos\left(3\theta - \varphi_3\right) + \cos\left(5\theta - \varphi_5\right)\right] \begin{bmatrix} \sin\left(\theta + \pi/3\right) \\ -\sin\left(\theta + \pi/3\right) \end{bmatrix} \\ &= \frac{\sqrt{3}}{6} \begin{bmatrix} \sin\left(-2\theta + \varphi_{+3}\right) + 2\sin\left(\varphi_- + \pi/3\right)\cos\left(4\theta - \varphi_+\right) + \sin\left(6\theta - \varphi_{-3}\right) \\ -\sin\left(-2\theta + \varphi_{+3}\right) - 2\sin\left(\varphi_- + \pi/3\right)\cos\left(4\theta - \varphi_+\right) - \sin\left(6\theta - \varphi_{-3}\right) \end{bmatrix} \end{aligned} \tag{7}$$

TABLE I
$F_{\Delta\varphi}$ UNDER DIFFERENT FAULTY PHASES FOR FAULT DETECTION

Faulty phase	*A*	*B*	*C*	*D*	*E*	*F*
$F_{\Delta\varphi}$	1			-1		

From (10), when the faulty phase is within (*A*, *B*, *C*), $\Delta\varphi$ is zero; when the faulty phase is within (*D*, *E*, *F*), $\Delta\varphi$ is π.

In practical detection, to eliminate the noise effect, we define

$$f_{\Delta\varphi} = \begin{cases} -1, & |\Delta\varphi - \pi| < \varepsilon \\ 1, & |\Delta\varphi - 0| < \varepsilon \\ 0, & \text{otherwise} \end{cases} \tag{11}$$

where ε is a preset value. Then, the moving average is applied as

$$F_{\Delta\varphi} = \frac{1}{T_\sigma}\int_{t-T_\sigma}^{t} f_{\Delta\varphi} dt \tag{12}$$

where T_σ is the period of the moving average. Table I presents $F_{\Delta\varphi}$ under different faulty phases. Thus, using $F_{\Delta\varphi}$, the fault in either (*A*, *B*, *C*) or (*D*, *E*, *F*) can be rapidly identified.

B. Fault Localization

After OPF either in (*A*, *B*, *C*) or (*D*, *E*, *F*) is identified, the second step is to locate in faulty phase using current harmonics in dq_{12} frame. We define the current i_l as

$$i_l \triangleq \begin{cases} \frac{(i_{d1,f}-i_{q2,f})(i_{q1,f}+i_{d2,f})}{(i_{d1,f}-i_{q2,f})^2+(i_{q1,f}+i_{d2,f})^2}, F_{\Delta\varphi}=1 \\ \frac{(i_{d1,f}+i_{q2,f})(i_{q1,f}-i_{d2,f})}{(i_{d1,f}+i_{q2,f})^2+(i_{q1,f}-i_{d2,f})^2}, F_{\Delta\varphi}=-1 \end{cases}. \tag{13}$$

The general form of the 2nd current harmonic in i_l is modeled as

$$i_L = I_L \cos(2\theta - \varphi_L) \tag{14}$$

where i_L is second harmonic component in i_l; I_L and φ_L are the amplitude and phase of i_L. In this letter, φ_L will be used to locate the faulty phase.

Considering phase *D* is open, substituting (3) into (2) yields

$$(i_{d1,f}+i_{q2,f})\cos(\theta-\pi/6)-(i_{q1,f}-i_{d2,f})\sin(\theta-\pi/6)=0. \tag{15}$$

Based on (15), one can derive

$$\begin{cases} i_{d1,f}+i_{q2,f} = N\sin(\theta-\pi/6) \\ i_{q1,f}-i_{d2,f} = N\cos(\theta-\pi/6) \end{cases} \tag{16}$$

where *N* is a coefficient. Based on (16), (17) can be derived as

$$\begin{cases} (i_{d1,f}+i_{q2,f})^2+(i_{q1,f}-i_{d2,f})^2 = N^2 \\ (i_{d1,f}+i_{q2,f})(i_{q1,f}-i_{d2,f}) = \frac{1}{2}N^2\cos(2\theta-5\pi/6) \end{cases}. \tag{17}$$

Substituting (17) into (13), we can obtain

$$i_L = i_l = \frac{1}{2}\cos(2\theta-5\pi/6). \tag{18}$$

Thus, when phase *D* is open, φ_L is equal to $5\pi/6$, that is

$$\varphi_L = 5\pi/6. \tag{19}$$

TABLE II
$F_{\varphi L}$ UNDER DIFFERENT FAULTY PHASES FOR FAULT LOCALIZATION

Faulty phase	*A*	*B*	*C*	*D*	*E*	*F*
φ_L	$\pi/2$	$-\pi/6$	$-5\pi/6$	$5\pi/6$	$\pi/6$	$-\pi/2$
$F_{\varphi L}$	1	2	3	-1	-2	-3

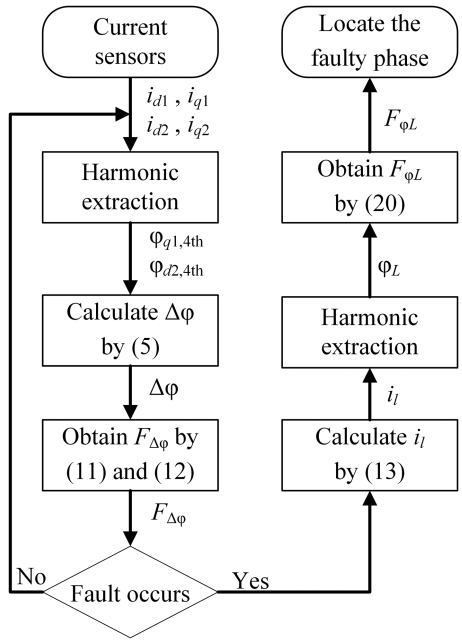

Fig. 2. Flowchart of the proposed two-step fault diagnostic method.

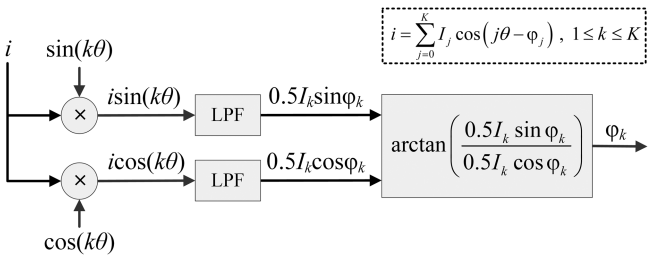

Fig. 3. Flowchart of harmonic extraction. LPF: low-pass filter.

Based on similar derivation, when the fault happens on other phases, the corresponding φ_L can be obtained, which is listed in Table II. For ease of observation, φ_L is rescaled by (20) and the results are listed in Table II as well

$$F_{\varphi L} = \begin{cases} \frac{7\pi/2-3\varphi_L}{2\pi}, & F_{\Delta\varphi}=1 \\ \frac{3\varphi_L-9\pi/2}{2\pi}, & F_{\Delta\varphi}=-1 \end{cases}. \tag{20}$$

From Table II, $F_{\varphi L}$ is capable of locating the fault.

C. Summary of the Two-Step Fault Diagnostic Method

The proposed fault diagnostic method is given in Algorithm I and Fig. 2. Firstly, $\varphi_{q1,4\text{th}}$ and $\varphi_{d2,4\text{th}}$ are extracted from the dq_{12} frame currents by using the harmonic extraction in Fig. 3.

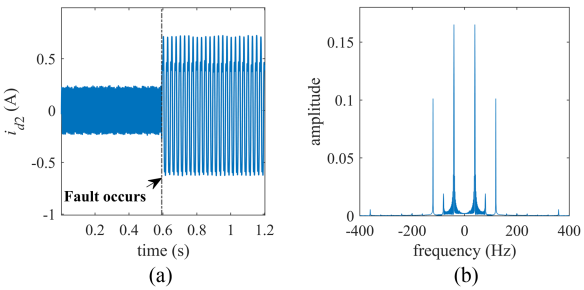

Fig. 4. High order harmonics and noise in the currents. (a) Waveforms of i_{d2}. (b) FFT results of i_{d2} under OPF.

TABLE III
RATED PARAMETERS OF THE TEST DT-PMSM

Rated speed	600 r/min	Number of poles	8
Rated torque	10 N•m	PM flux linkage	0.1 Wb•turn
Rated current	8 A	Winding resistance	0.6 Ω

Algorithm I: Two-Step Fault Diagnosis Using Harmonic Components

Fault detection stage

1. Extract $\varphi_{q1,4\text{th}}$ and $\varphi_{d2,4\text{th}}$ from i_{q1} and i_{d2};
2. Calculate $\Delta\varphi$ by (5);
3. Obtain $F_{\Delta\varphi}$ by (11) and (12);
4. Detect whether the fault occurs and locate the faulty winding.

Fault localization stage

1. Calculate i_l by (13);
2. Extract φ_L from i_l;
3. Obtain $F_{\varphi L}$ by (20);
4. Locate the faulty phase.

Then, $\Delta\varphi$ is calculated by (5) and $F_{\Delta\varphi}$ is obtained from (11) and (12). Based on Table I, detect whether the fault occurs in (*A*, *B*, *C*) or (*D*, *E*, *F*). Finally, calculate i_l by (13) and extract φ_L to compute $F_{\varphi L}$ using (20). Based on Table II, locate the faulty phase.

Remark: When OPF occurs, high order harmonics and high frequency noise will be introduced in the currents, as shown in Fig. 4. In the existing methods, the noise and harmonics could affect their diagnostic performance and reliability as well as the diagnostic time. However, in the proposed method, the current harmonics are extracted using the harmonic extraction, which can effectively suppress the effect of noise and other harmonics.

IV. EXPERIMENTAL INVESTIGATION

To validate the proposed diagnostic method, experiments are conducted on a test motor, as shown in Fig. 5. And the rated parameters are given in Table III. On one hand, a small ε could suppress the noise effectively, but it will increase the diagnostic time. On the other hand, a large ε will result in more noise in the indicator and thus worse diagnostic reliability. Thus, in this letter, ε is experimentally selected as 10°, which can reduce the effect of noise and achieve fast diagnosis. Similarly, T_σ in (12) is set to 0.125 fundamental period, which can improve the detection speed. When the motor operates online, the currents in dq_{12} frame are measured. Then, $F_{\Delta\varphi}$ is extracted from currents and used to detect OPF. When the fault is detected, $F_{\varphi L}$ is extracted from 2nd current harmonic. Based on the value of $F_{\varphi L}$, the faulty phase is located exactly.

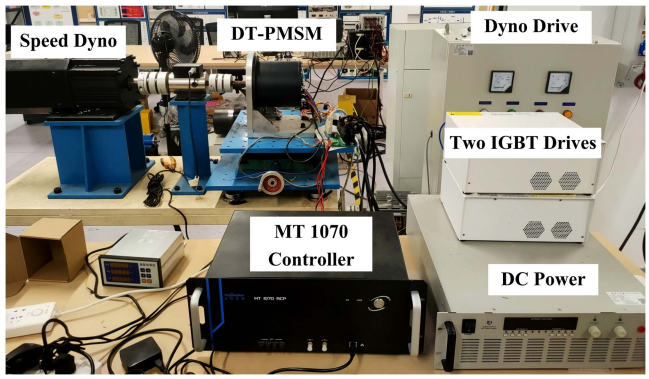

Fig. 5. Experimental setup for fault diagnosis.

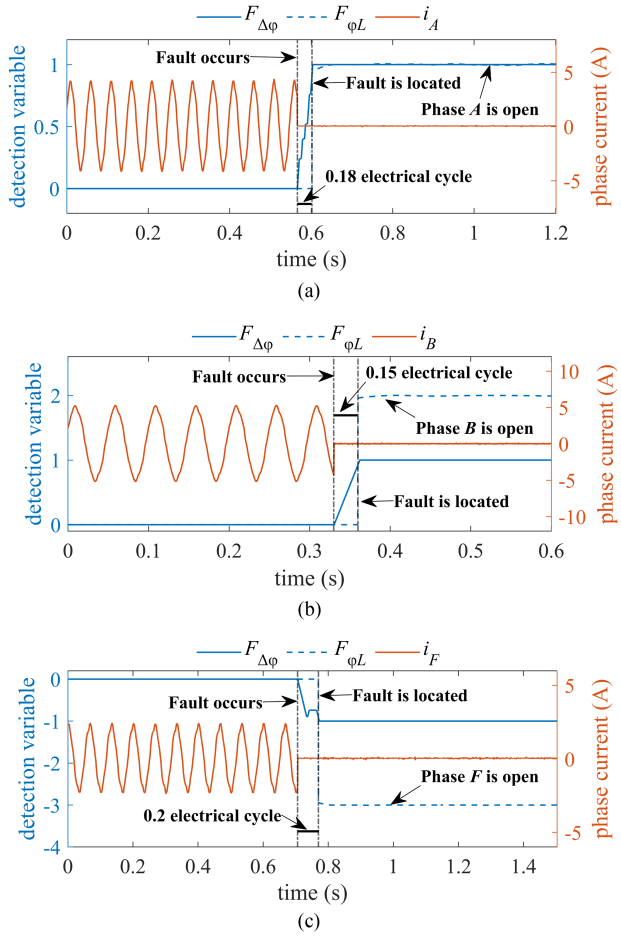

Fig. 6. Fault diagnostic results under steady state. (a) Phase *A* is open. (b) Phase *B* is open. (c) Phase *F* is open.

A. Test Results and Comparison Under Various Conditions

Fault diagnostic results under steady state are shown in Fig. 6. In Fig. 6(a), the motor operates at 300 r/min with phase *A* open

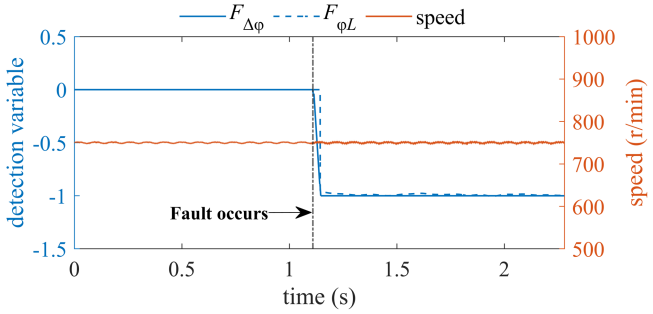

Fig. 7. Fault diagnostic results at a high speed of 750 r/min with phase D open.

when $i_{d1} = 0$ and $i_{q1} = 4$ A. One electrical cycle is 0.2 s. At 0.566 s, the motor switches from healthy state to OPF. At 0.602 s, $F_{\Delta\varphi}$ grows to 1. Almost at the same time, $F_{\varphi L}$ grows to 1, indicating phase A is under OPF. The diagnostic time is 0.036 s (about 0.18 electrical cycle). In Fig. 6(b), the motor operates at 300 r/min with phase B open when $i_{d1} = 0$ and $i_{q1} = 5$ A. One electrical cycle is 0.2 s. At 0.330 s, the fault occurs. At 0.360 s, $F_{\Delta\varphi}$ and $F_{\varphi L}$ change to 1 and 2, indicating phase B is under OPF. The diagnostic time is 0.030 s (about 0.15 electrical cycle). In Fig. 6(c), at 225 r/min, phase F is open when $i_{d1} = -1$ A and $i_{q1} = 2$ A. One electrical cycle is 0.27 s. At 0.711 s, the fault occurs. At 0.765 s, $F_{\Delta\varphi}$ and $F_{\varphi L}$ change to -1 and -3, indicating phase F is under OPF. The diagnostic time is 0.054 s (about 0.2 electrical cycle). The results validate the proposed method can diagnose OPFs effectively and quickly.

Fig. 7 presents the diagnostic results with phase D open when $i_{d1} = 0$ and $i_{q1} = 2$ A at a higher speed of 750 r/min. When the fault occurs, both $F_{\Delta\varphi}$ and $F_{\varphi L}$ change to -1, indicating phase D is open. The indicators are designed based on second and fourth harmonics due to the fault. Even under high speeds, these harmonics are still existing and can be used for fault diagnosis. The bandwidths of current sensors are sufficient to measure the second and fourth harmonics at high speeds. Thus, the proposed method can achieve the accurate fault diagnosis at high speeds.

Fault diagnostic results under operating condition change are shown in Fig. 8, where phase D is open. In Fig. 8(a), the speed changes from 225 to 450 r/min when $i_{d1} = -1$ A and $i_{q1} = 2$ A. Before 1.90 s, both $F_{\Delta\varphi}$ and $F_{\varphi L}$ are -1, indicating phase D is open. From 1.90 to 2.64 s, the speed changes. During the test, $F_{\Delta\varphi}$ and $F_{\varphi L}$ remain unchanged and almost have no fluctuation. In Fig. 8(b), i_{q1} changes from 2 to 3 A when i_{d1} is fixed to -1 A at 300 r/min. At 0.67 s, i_{q1} changes, and $F_{\Delta\varphi}$ and $F_{\varphi L}$ remain unchanged without fluctuation. Hence, the proposed method is robust to the operating condition change. When the operating condition changes, motor parameters, such as inductances, will vary nonlinearly due to saturation. The proposed method does not require motor parameters and thus it is robust to parameter change, which is verified by the results in Fig. 8.

Fig. 9 presents the fault diagnostic results under different bandwidths of the current regulator with phase D open when $i_{d1} = 0$ and $i_{q1} = 2$ A at 300 r/min. In Fig. 9(a), the proportion coefficient K_p is 9.5 and the integral coefficient K_i is 500. In Fig. 9(b), K_p is 20 and K_i is 700. It can be observed that

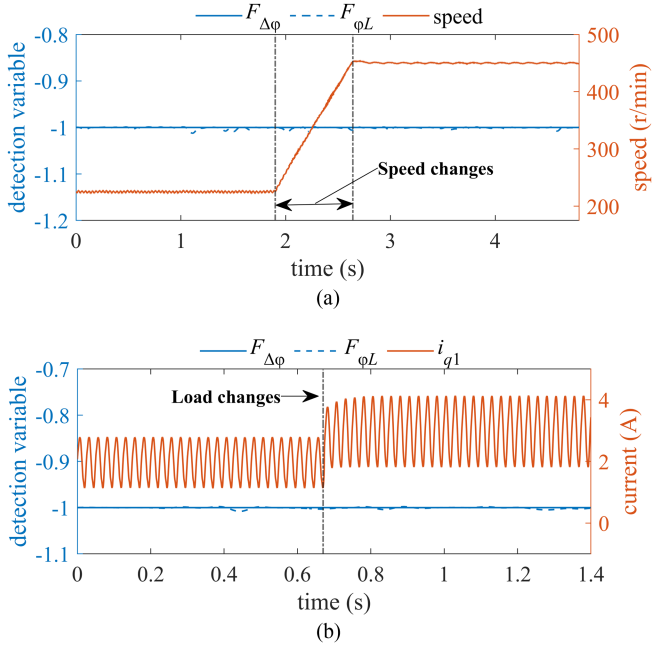

Fig. 8. Fault diagnostic results under operating condition change with phase D open. (a) Speed changes. (b) Load changes.

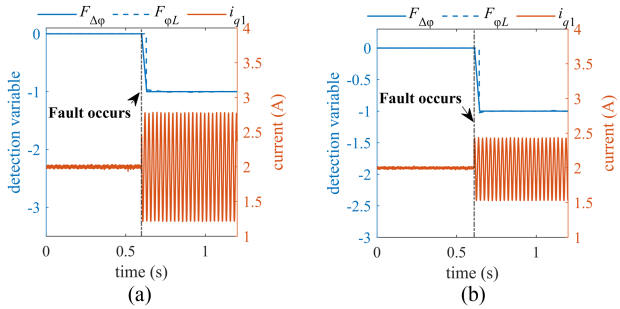

Fig. 9. Fault diagnostic results under different bandwidths of the current regulator with phase D open. (a) $K_p = 9.5$, $K_i = 500$. (b) $K_p = 20$, $K_i = 700$.

the proposed method can accurately locate the fault, which is not affected by the bandwidths of the current regulators. The indicators are designed based on fault induced harmonics, which are not affected by the current regulators. Thus, the proposed method is robust to bandwidths of the current regulators.

The proposed method is compared with M1 [13], M2 [14], and M3 [17]. In M1, a preset threshold is used to detect whether the fault occurs and then the angle between the currents in xy frame is used to locate the faulty phase. Under $i_d = 0$ control, M2 divides six phase currents into d-axis and residual components, and uses the ratios of these components as fault indicators. Through transformation, M3 obtains axis currents in six reconstructed frames and employs the ratio combinations of axis currents to achieve the fault diagnosis. Table IV gives the comparison results in terms of diagnostic time, number of detection variables, computation efficiency, robustness and applicable control strategy. Compared with M1–M3, the proposed method achieves faster diagnostic speed using high order harmonics. Compared with M2 and M3, the proposed method needs less

TABLE IV
COMPARISONS OF DIFFERENT DIAGNOSTIC METHODS

Methods	Diagnostic time*	Detection variables	Computation efficiency	Robust-ness	Control strategy
M1 [13]	1	2	Better	Low	i_d=0
M2 [14]	≤ 0.25	6	Worse	Medium	i_d=0
M3 [17]	≤ 0.25	6	Worse	High	Universal
Proposed method	≤ 0.2	2	Better	High	Universal

* The unit of diagnostic time is electrical cycle.

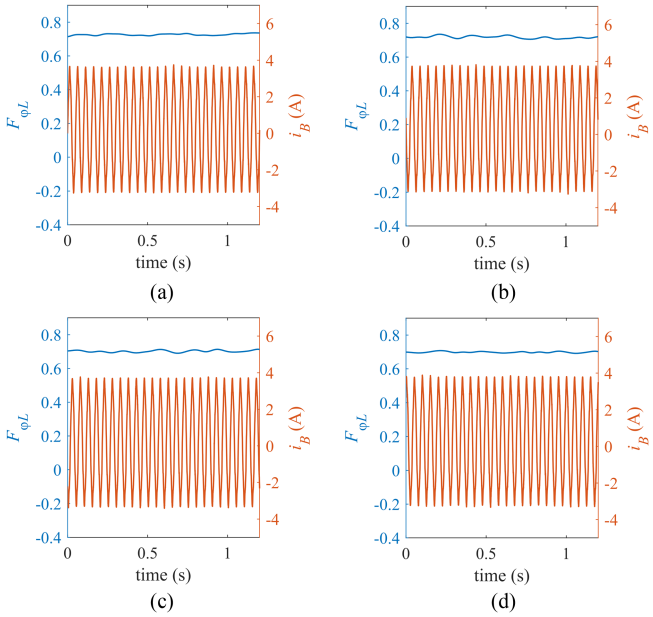

Fig. 10. Fault diagnostic results under different types of CSF in phase B. (a) $K_a = 1.2$, $K_b = 0.5$. (b) $K_a = 1.2$, $K_b = 0.8$. (c) $K_a = 1.3$, $K_b = 0.5$. (d) $K_a = 1.3$, $K_b = 0.8$.

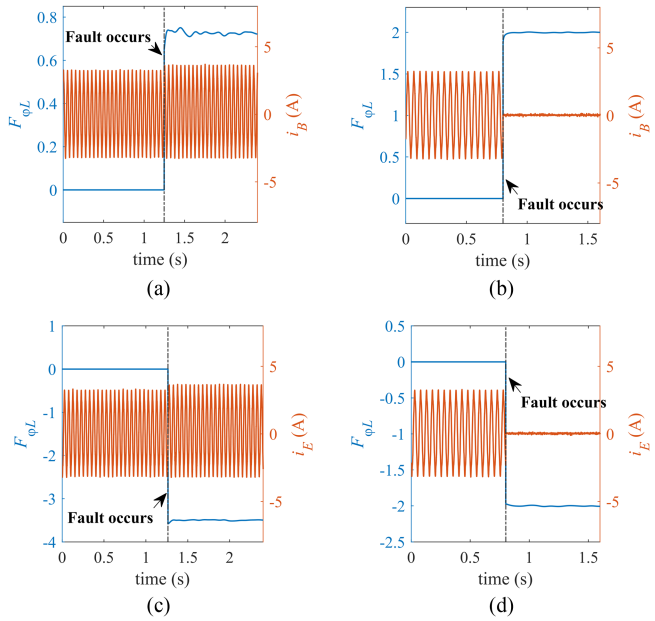

Fig. 11. Fault diagnostic results under different fault types. (a) CSF in phase B. (b) OPF in phase B. (c) CSF in phase E. (d) OPF in phase E.

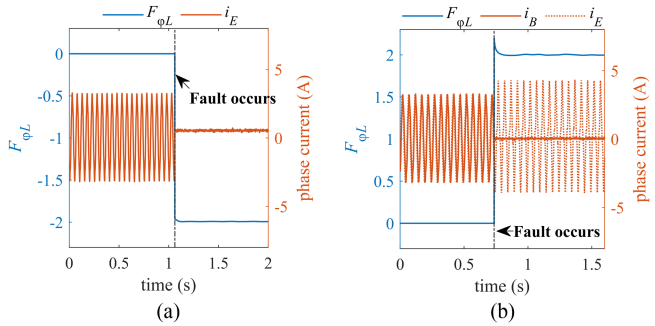

Fig. 12. Fault diagnostic results under multiple faults. (a) OPF and CSF in phase E. (b) OPF in phase B and CSF in phase E.

detection variables and avoids additional transformation, which can improve the computation efficiency significantly. Moreover, the proposed method is robust to harmonics, noise and operating condition change. And the proposed method is applicable to various control strategies, while M1 and M2 limit to $i_d = 0$ control. Hence, the proposed method presents better diagnostic performance.

B. Test Results Under the Influence of Other Faults

According to [24], among various faults, current sensor fault (CSF) could introduce 1st and 2nd harmonics in the dq_{12} currents. Here, CSF means during calculating the current using current sensor output, the scaling K_a and offset K_b are not accurate.

To investigate the fault separation capability of the proposed method, tests are conducted under different types of CSF. In these tests, the operating condition is set to $i_{d1} = 0$ and $i_{q1} = 3$ A at 300 r/min. Fig. 10 presents the results when four types of CSF happen to phase B (four scaling and offset errors are studied). Four types of CSF are: $K_a = 1.2$, $K_b = 0.5$; $K_a = 1.2$, $K_b = 0.8$; $K_a = 1.3$, $K_b = 0.5$; and $K_a = 1.3$, $K_b = 0.8$ (real $K_a = 1$, real $K_b = 0$). It can be observed from Fig. 10 that the developed indicator $F_{\varphi L}$ always remains at 0.7. However, when OPF happens to phase B, $F_{\varphi L}$ is 2. Hence, $F_{\varphi L}$ can effectively separate the CSF and OPF. Fig. 11 presents the results when CSF happens to other phases with $K_a = 1.2$ and $K_b = 0.5$. It can be observed that when CSF happens to different phases, the value of $F_{\varphi L}$ is different, which is also different from the OPF. For instance, $F_{\varphi L}$ is -3.5 with CSF in phase E, while $F_{\varphi L}$ is -2 with OPF in phase E. Similar results can be found on other phases. Hence, the proposed method can effectively separate OPF and CSF.

To validate the sensitivity of the proposed method, the OPF diagnosis is conducted under the both OPF and CSF. In this test, the currents are set to $i_{d1} = 0$ and $i_{q1} = 3$ A and the motor speed is 300 r/min, where OPF and CSF occur simultaneously. The results are shown in Fig. 12. In Fig. 12(a), OPF happens in phase E, $F_{\varphi L}$ is -2, which indicates OPF is accurately located in phase E. In Fig. 12(b), OPF happens in phase B, $F_{\varphi L}$ is 2, which indicates OPF is accurately located in phase B. It can be

seen that even under the influence of other faults, the proposed method can still accurately locate the OPF, which validates the robustness of the proposed method.

V. Conclusion

In this letter, a fast and efficient two-step OPF diagnostic method is proposed using harmonic components. Through high order current harmonics, the fault is detected and located quickly. The two-step strategy divides the diagnosis into detection and localization, which can improve the computation efficiency. Besides, the harmonic extraction can reduce the effect of harmonics and noise. As the detection variables are independent of motor parameters and operating conditions, the proposed method is robust. Finally, the experiments and comparisons validate the performance of the proposed method.

Appendix I

$$\boldsymbol{T}_{VSD}=\frac{1}{3}\begin{bmatrix}1 & -\frac{1}{2} & -\frac{1}{2} & \frac{\sqrt{3}}{2} & -\frac{\sqrt{3}}{2} & 0\\ 0 & \frac{\sqrt{3}}{2} & -\frac{\sqrt{3}}{2} & \frac{1}{2} & \frac{1}{2} & -1\\ 0 & \frac{\sqrt{3}}{2} & -\frac{\sqrt{3}}{2} & -\frac{1}{2} & -\frac{1}{2} & 1\\ -1 & \frac{1}{2} & \frac{1}{2} & \frac{\sqrt{3}}{2} & -\frac{\sqrt{3}}{2} & 0\end{bmatrix},$$

$$\boldsymbol{T}_{R}=\begin{bmatrix}\cos\theta & \sin\theta & 0 & 0\\ -\sin\theta & \cos\theta & 0 & 0\\ 0 & 0 & \cos\theta & \sin\theta\\ 0 & 0 & -\sin\theta & \cos\theta\end{bmatrix}. \tag{21}$$

Appendix II

Due to the structure of the three-phase winding, when D is open, define the harmonics in phases A, B, and C as

$$\boldsymbol{i}_{s,3,5}=\begin{bmatrix}I_3\cos(3\theta-\varphi_3)+I_5\cos(5\theta-\varphi_5)\\ I_3\cos(3\theta-\varphi_3-2\pi/3)+I_5\cos(5\theta-\varphi_5+2\pi/3)\\ I_3\cos(3\theta-\varphi_3+2\pi/3)+I_5\cos(5\theta-\varphi_5-2\pi/3)\\ \mathbf{0}_{3\times1}\end{bmatrix}. \tag{22}$$

Substituting (22) into (2), we can obtain

$$\begin{bmatrix}i_{q1,2,4,6}\\ i_{d2,2,4,6}\end{bmatrix}=\frac{1}{2}\begin{bmatrix}I_3\sin(2\theta-\varphi_3)-I_5\sin(6\theta-\varphi_5)\\ I_3\sin(2\theta-\varphi_3)-I_5\sin(6\theta-\varphi_5)\end{bmatrix}. \tag{23}$$

In (23), there is no 4th harmonic. Hence, in (6), the harmonics in phases A, B, and C do not affect the results in (8).

References

[1] P. P. Das, S. Satpathy, and S. Bhattacharya, "An online open-circuit fault diagnosis technique for three-level inverter-fed six-phase PMSM drives," *IEEE Trans. Power Electron.*, vol. 39, no. 11, pp. 14974–14987, Nov. 2024.

[2] R. Duan, L. Wu, Z. Lyu, H. Zhan, and P. Song, "Harmonic subspace signature-based detection and localization of interturn short-circuit fault for dual three-phase PMSM with VSD scheme," *IEEE Trans. Transp. Electrific.*, vol. 10, no. 4, pp. 9652–9664, Dec. 2024.

[3] J. Hang, X. Wang, W. Li, and S. Ding, "Interturn short-circuit fault diagnosis and fault-tolerant control of DTP-PMSM based on subspace current residuals," *IEEE Trans. Power Electron.*, vol. 40, no. 2, pp. 3395–3404, Feb. 2025.

[4] Y. Yu, S. Yang, X. Zhang, Y. Qu, and G. Qin, "Interturn short-circuit fault diagnosis and localization of PMSM based on current trajectory," *IEEE Sensors J.*, vol. 25, no. 1, pp. 1155–1163, Jan. 2025.

[5] Z. Song, Y. Jia, and C. Liu, "Open-phase fault-tolerant control strategy for dual three-phase permanent magnet synchronous machines without controller reconfiguration and fault detection," *IEEE Trans. Power Electron.*, vol. 38, no. 1, pp. 789–802, Jan. 2023.

[6] S. Xu, X. Chen, W. Yang, F. Liu, and Y. Chai, "Current sensor incipient fault diagnosis in PMSM drive systems using novel interval sliding mode observer," *IEEE Trans. Instrum. Meas.*, vol. 73, 2024, Art. no. 3508211.

[7] W. Huang, J. Du, W. Hua, K. Bi, and Q. Fan, "A hybrid model-based diagnosis approach for open-switch faults in PMSM drives," *IEEE Trans. Power Electron.*, vol. 37, no. 4, pp. 3728–3732, Apr. 2022.

[8] L. Kong, Y. Mao, T. Zhang, X. Chen, Z. Wang, and X. Wang, "Online data-driven diagnosis for common electrical and sensor faults in dual three-phase PMSM drives," *IEEE Trans. Instrum. Meas.*, vol. 74, 2025, Art. no. 2507510.

[9] J. Hang, X. Shu, S. Ding, and Y. Huang, "Robust open-circuit fault diagnosis for PMSM drives using wavelet convolutional neural network with small samples of normalized current vector trajectory graph," *IEEE Trans. Ind. Electron.*, vol. 70, no. 8, pp. 7653–7663, Aug. 2023.

[10] L. Jin, X. Wang, Y. Mao, L. Lu, and Z. Wang, "Online attribute matching based few-sample data-driven diagnosis of electrical faults in PMSM drive," *IEEE Trans. Power Electron.*, vol. vol. 39, no.no. 2, pp. 2620–2631, Feb. 2024.

[11] L. Jin, Y. Mao, X. Wang, L. Lu, and Z. Wang, "Online data-driven fault diagnosis of dual three-phase PMSM drives considering limited labeled samples," *IEEE Trans. Ind. Electron.*, vol. 71, no. 7, pp. 6797–6808, Jul. 2024.

[12] X. Wu et al., "A fast and robust diagnostic method for multiple open-circuit faults of voltage-source inverters through line voltage magnitudes analysis," *IEEE Trans. Power Electron.*, vol. 35, no. 5, pp. 5205–5220, May 2020.

[13] P. Shi, X. Wang, X. Meng, M. He, Y. Mao, and Z. Wang, "Adaptive fault-tolerant control for open-circuit faults in dual three-phase PMSM Drives," *IEEE Trans. Power Electron.*, vol. 38, no. 3, pp. 3676–3688, 2023.

[14] L. Guo, K. Wang, T. Wang, R. Cao, and F. Li, "Open-circuit fault diagnosis for dual three-phase permanent magnet machine considering nonideal condition," *IEEE Trans. Ind. Electron.*, vol. 71, no. 9, pp. 10288–10296, Sep. 2024.

[15] X. Zheng, X. Zhang, X. Liu, and X. Yuan, "A new signal-based diagnosis method for current sensor and open-circuited faults of a nine-phase open-end winding PMSM," *IEEE Trans. Transport. Electrific.*, vol. 11, no. 1, pp. 1214–1222, Feb. 2025.

[16] W. Wang, Y. Mao, P. Cui, J. Fu, W. Hua, and M. Cheng, "Double normalization fault diagnosis method for open-circuit faults of PMSM drives," *IEEE Trans. Power Electron.*, vol. 39, no. 9, pp. 11613–11624, Sep. 2024.

[17] Z. Zhou and H. Yang, "An efficient and robust open-phase fault diagnosis scheme for dual three-phase PMSMs drive using axis transformation," *IEEE Trans. Transport. Electrific.*, to be published, doi: 10.1109/TTE.2025.3533951.

[18] Y. Hu, Z. Q. Zhu, and M. Odavic, "Comparison of two-individual current control and vector space decomposition control for dual three-phase PMSM," *IEEE Trans. Ind. Appl.*, vol. 53, no. 5, pp. 4483–4492, May 2017.

[19] H. Hu et al., "Fast online fault diagnosis for PMSM based on adaptation model," *IEEE Sensors J.*, vol. 24, no. 15, pp. 24319–24327, Aug. 2024.

[20] Z. Chen, D. Liang, S. Jia, and S. Yang, "Model-based data normalization for data-driven PMSM fault diagnosis," *IEEE Trans. Power Electron.*, vol. 39, no. 9, pp. 11596–11612, Sep. 2024.

[21] X. Feng, B. Wang, Z. Wang, W. Hua, and M. Cheng, "Diagnosis and Identification of common electrical faults in PM machine drives," *IEEE Trans. Power Electron.*, vol. vol. 39, no.no. 10, pp. 13686–13695, Oct. 2024.

[22] B. Liu, T. Shi, G. Zhang, W. Chen, and C. Xia, "Open-circuit fault diagnosis method for inverter in PMSM drives considering closed-loop regulation," *IEEE J. Emerg. Sel. Topics Power Electron.*, vol. 12, no. 5, pp. 5298–5310, Oct. 2024.

[23] W. Zhao, Y. Chen, T. Tao, S. Ding, and T. Zhang, "Open-phase fault and current sensor fault diagnosis based on spatial distributions of phase currents for dual three-phase PMSM drives," *IEEE Trans. Ind. Electron.*, vol. 72, no. 5, pp. 4375–4388, May 2025.

[24] A. Wireko-Brobby, Y. Hu, G. Wang, C. Gong, W. Lang, and Z. Zhang, "Analysis of the sources of error within PMSM-based electric powertrains—A review," *IEEE Trans. Transport. Electrific.*, vol. 10, no. 3, pp. 6370–6406, Sep. 2024.